Transportation Geotechnics 55 (2025) 101652

Contents lists available at ScienceDirect

Transportation Geotechnics

journal homepage: www.elsevier.com/locate/trgeo

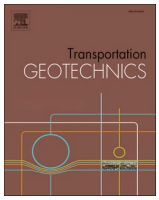

Prediction of future railway ballast tamping requirements

C. Charoenwong [a,*], D.P. Connolly [a], T. Wang [b], K. Liu [b], P. Alves Costa [c], A. Romero [d], P. Galvín [d,e]

[a] School of Civil Engineering, University of Leeds, UK
[b] School of Civil Engineering, Southwest Jiaotong University, Chengdu 610031, China
[c] CONSTRUCT-FEUP, Department of Civil Engineering, Faculty of Engineering, University of Porto, Rua Dr. Roberto Frias s/n, 4200-465 Porto, Portugal
[d] Escuela Técnica Superior de Ingeniería, Universidad de Sevilla, Camino de los Descubrimientos s/n, 41092 Sevilla, Spain
[e] Laboratory of Engineering for Energy and Environmental Sustainability, Universidad de Sevilla, Camino de los Descubrimientos s/n, 41092 Sevilla, Spain

ARTICLE INFO

Keywords:
Railway ballast differential settlement
Machine tamping intervals
Track geometry deterioration
Ballast fouling
Ballast moisture content
Railway track renewal

ABSTRACT

This paper presents a numerical framework for predicting future railway ballast tamping requirements under varying operational and environmental conditions. The approach integrates an empirical ballast settlement model, derived from large-scale laboratory tests, into a dynamic track-ground interaction framework using the 2.5D Finite Element Method. It is capable of capturing differential settlement and track geometry deterioration considering different types of ballast fouling material, varying levels of ballast moisture content, train speed and traffic volume. Track geometry profiles are updated iteratively after each axle passage, enabling condition-based assessment of future tamping needs. First the model is calibrated using historical track geometry data from an operational railway line. Following calibration, an analysis is performed to study the effect of different moisture levels and types of ballast fouling material (sand, coal and abrasion-induced fines) on track geometry degradation and ultimately future tamping requirements. Next, to understand the effect of different possible track renewal strategies on future tamping requirements, the effects of increasing the rail section and adding under sleeper pads are compared. Results indicate that moisture content, speed, and traffic volume are dominant factors governing tamping frequency. While the type of fouling material and the proposed renewal strategies have a comparatively moderate effect, their influence remains non-negligible. These findings highlight the importance of maintaining adequate track drainage and implementing measures to control the type and extent of ballast fouling.

Introduction

Railway ballast on-track tamping machines use lifting and squeezing to correct vertical and lateral track deviations, thus restoring track geometry[1–3]. Although tamping aims to correct track geometry and restore support conditions by rearranging ballast particles beneath the sleepers, it typically does not fully restore the original track quality[3,4]. The effectiveness of tamping, referred to as tamping recovery, often declines with repeated interventions due to cumulative ballast deterioration and damage caused by successive tamping actions[5]. Nevertheless, regularly scheduled tamping remains essential for maintaining track geometry. This helps ensure passenger safety and comfort, reduces derailment risks, and supports efficient train operations.

Given the high resource demands and diminishing effectiveness of repeated tamping, accurately predicting future tamping requirements is important. Reliable predictions are useful for both optimising tamper resource allocation, which involves efficient use of machines, personnel, and track access windows, and for understanding the implications of long-term maintenance and renewal strategies. Proactive planning based on predictive models enables infrastructure managers to reduce lifecycle costs and minimise service disruptions by balancing the frequency and timing of tamping with alternative treatments such as ballast cleaning or complete track renewal.

Accurate prediction depends on an understanding of the factors influencing track geometry deterioration. Key parameters such as train speed, traffic volume, ballast fouling, and moisture presence have a significant impact on trackbed deterioration which affects tamping requirements. For example, higher train speeds introduce greater dynamic forces that accelerate geometry degradation and increase deviatoric stress within the ballast, thereby necessitating more frequent tamping

* Corresponding author.
E-mail address: c.charoenwong@leeds.ac.uk (C. Charoenwong).

https://doi.org/10.1016/j.trgeo.2025.101652
Received 28 May 2025; Received in revised form 14 July 2025; Accepted 25 July 2025
Available online 25 July 2025

[6]. Likewise, increased traffic volume, measured in million gross tons (MGT), imposes more load cycles, leading to faster ballast settlement and reduced tamping interval. Ballast fouling, indicated by a higher Fouling Index (FI), resulting from fine particle contamination, impedes drainage and retains moisture, accelerating settlement and necessitating more frequent tamping interventions[7,8]. Moreover, the combined effect of fouling and moisture presence exacerbates ballast particle rearrangement and settlement rates, further decreasing the interval between necessary tamping operations[9]. While the importance of these factors is widely acknowledged, their interactions and cumulative impacts on tamping intervals have not yet been thoroughly quantified or understood, emphasising the need for further investigation.

To meet this need, numerical models have become increasingly important in understanding railway ballast behaviour and predicting maintenance needs, including the scheduling of tamping operations. While tamping restores track geometry by filling voids and compacting the ballast bed, determining the best time for intervention remains complex and cost-sensitive[4]. Numerical modelling provides a way to simulate ballast behaviour and predict when tamping might be required. For example, the Discrete Element Method (DEM) has been widely applied for simulating ballast behaviour during tamping[10–13]. These models provide insights into the mechanics of tamping at the particle level, focusing particularly on the penetration and withdrawal of tamping tines and ballast breakage. Despite these advancements, existing DEM simulations typically address isolated tamping events and face computational limitations when modelling the large-scale ballast disturbances associated with repeated tamping cycles and cyclic train loading. Consequently, these models often fail to adequately capture the cumulative and path-dependent behaviour of ballast, limiting their predictive accuracy for optimal tamping scheduling [4,14].

In response, mechanics-based models have emerged as an alternative to represent long-term settlement processes, track geometry deterioration and maintenance scheduling[15]. For example, various methods have been proposed to predict differential track settlement due to train loading, typically employing iterative simulations of train passages coupled with settlement models that account for variations in track geometry[16–19]. However, accurately capturing the complexities of cyclic loading, including detailed representation of 3D dynamic stress fields, remains computationally demanding[20–24]. Railway settlement prediction generally follows either constitutive approaches, which offer detailed yet computationally intensive simulations requiring extensive material data[25–28], or empirical methods, which use fewer parameters to efficiently and effectively replicate observed settlement behaviour[29–32].

In contrast to these prior approaches, this paper presents a novel approach for predicting track settlement and tamping interventions based on evolving track conditions. An empirical equation, derived from laboratory tests on fouled ballast under both dry and wet conditions, is integrated into a numerical framework that simulates differential track settlement in response to varying fouling and moisture levels. Unlike traditional models, this approach incorporates a dynamic representation of train-track interaction, vehicle response, and the propagation of three-dimensional stress fields within the track structure. To ensure computational efficiency while preserving physical accuracy, the model employs an equivalent-linear 3D wavenumber finite element method linked with the empirical settlement function. A key innovation lies in the continuous update of vertical track irregularities after each load cycle, allowing for a detailed evaluation of track quality degradation over time. Tamping interventions are incorporated into the model based on representative maintenance criteria, triggered either when track geometry deterioration reaches a predefined quality threshold or at scheduled preventive intervals, reflecting standard industry practice. The model also accounts for the immediate improvement in track geometry following tamping, followed by a short-term phase of accelerated settlement as the ballast re-stabilises under traffic loading. This enables a more realistic simulation of track behaviour post-maintenance and supports a condition-based tamping strategy that enhances maintenance precision and long-term infrastructure performance.

The analyses presented in this study examine the effects of operational and material parameters on tamping intervals under fouled ballast conditions. Specifically, the influence of moisture content (0 %, 3 %, and 6 %) and train speeds (130, 160, and 200 km/h) is investigated. Variations in annual traffic volume, represented as 17.5 and 35.0 million gross tonnes per annum (MGTPA), are also considered. The study further explores the impact of different types of ballast fouling material. In addition, three renewal strategies are evaluated: 1) a standard track design with 56 kg/m rail, 2) the same standard track design but with a heavier 60 kg/m rail (UIC60), 3) the same standard track design but with a heavier 60 kg/m rail and Under Sleeper Pads (USPs). These renewal strategies are assessed for their potential to extend tamping intervals and improve long-term track performance.

Numerical modelling

Model overview

To predict differential settlement and tamping interventions for railway tracks, the modelling employs a 2.5D Finite Element Method incorporating Perfectly Matched Layers (FEM-PML), solved through a hybrid approach across both frequency-wavenumber and time–space domains. This wavenumber finite element methodology offers a computationally efficient means of addressing three-dimensional problems by discretising two dimensions via finite element theory and analytically solving the third. Consequently, it is suitable for structures with invariant geometry and material properties along one dimension, such as railways, highways, and tunnels. In this study, the method is applied to tangent track sections only, with no consideration of stiffness transitions such as those found at bridges, tunnels, or switches.

Assuming linear and elastic structural behaviour, the equations of motion are resolved in the wavenumber-frequency domain. Variables are transformed into this domain using a double Fourier transform concerning the train's direction of travel (x-direction) and time (t). Although discrete sleepers can be explicitly simulated using a full 3D model, the 2.5D method approximates sleeper discontinuities by employing modified anisotropy. Following [33,34], sleepers are represented as continuous, orthotropic elements reflecting actual sleeper properties in the cross-sectional plane but possessing zero stiffness longitudinally. This simplification yields acceptable accuracy within the investigated frequency range [35].

To ensure the capture of critical wave phenomena within the frequency domain of interest, the wavenumber is restricted to a maximum of 10 rad/m[36], which corresponds to a minimum wavelength of approximately 0.63 m. This domain, extending from −10 to +10 rad/m, is discretised using 1024 sampled points, balancing computational efficiency and precision in resolving integrand peaks.

The flowchart of the modelling process is illustrated in Fig. 1. In this approach, transfer functions are precomputed, and the iterative process addresses the progressive prediction of the track settlement. The use of transfer functions enhances computational efficiency by enabling rapid updates to the track geometry profile after each loading event, followed by the determination of the corresponding track geometry standard deviation (SD) over a desired track length. Previous studies [37,38] have examined the impact of varying frequencies of track geometry updates on differential settlement. While updating the geometry after every axle passage increases computational demands, insufficient update frequency can result in inaccuracies by failing to adequately account for the cumulative effects of train-track interactions. This can, in turn, affect the accuracy of predictions and the timing of required tamping interventions.

The initial phase of the simulation involves calculating the 3D elastodynamic response and geostatic stresses within the track and subgrade, representing the at-rest stress conditions prior to loading. An

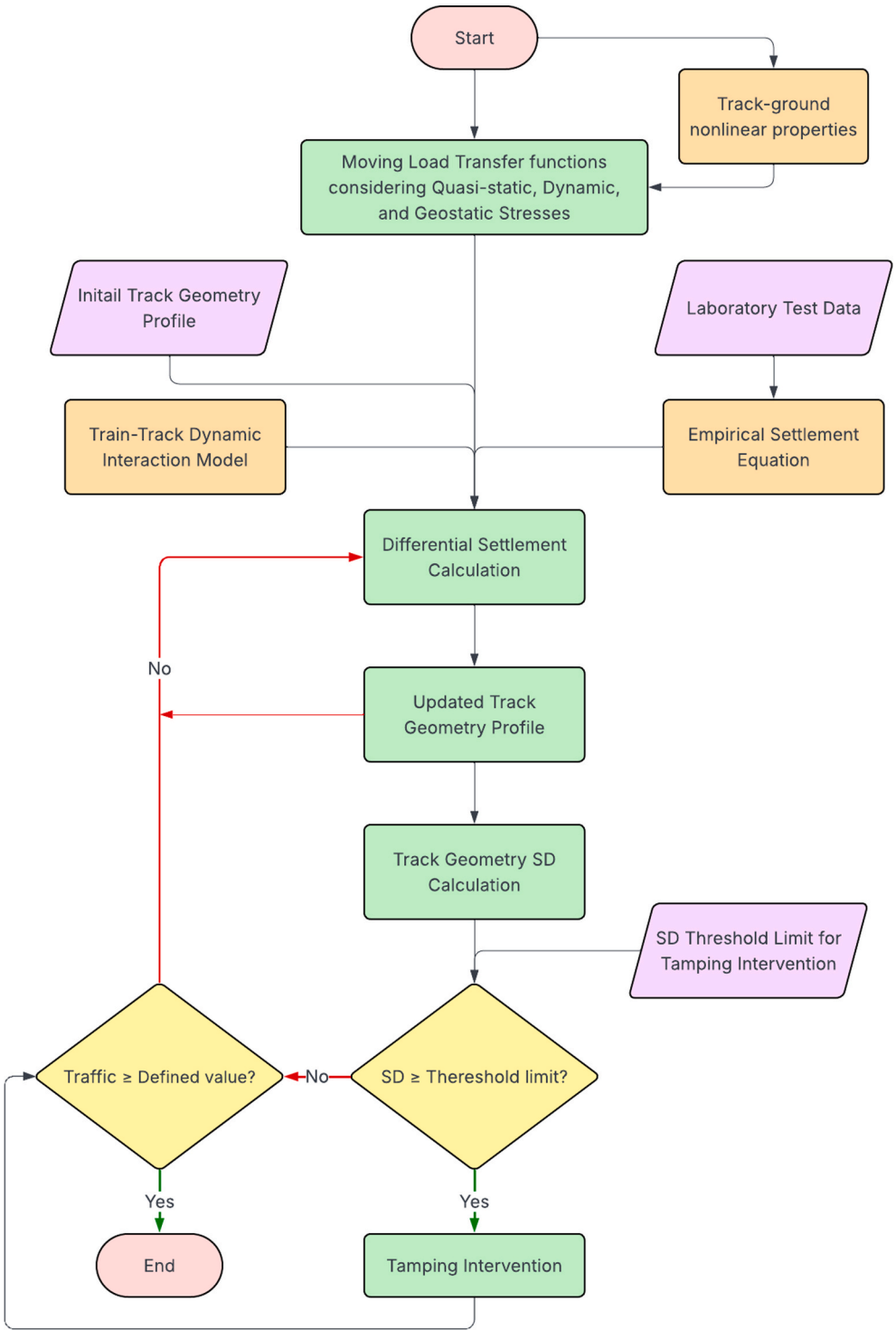

Fig. 1. Flowchart of the modelling process.

example of the response propagating from the rail into the supporting track-ground structure is illustrated is Fig. 2. The moving load transfer functions, derived in the frequency–wavenumber domain, incorporate equivalent nonlinear stiffness and damping properties of the track and ground. These properties are obtained through a strain-dependent iterative procedure and are held constant during the transfer function computation to preserve computational efficiency while capturing the essential effects of nonlinear behaviour in the track and ground. The transfer functions refer to the precomputed 3D elastodynamic response of the track–ground system in the frequency–wavenumber domain. These include the moving load transfer functions, which capture the stress response due to quasi-static and dynamic loading, and are derived using the 2.5D FEM-PML method. The detailed formulation and implementation for the transfer functions follow the methods described in

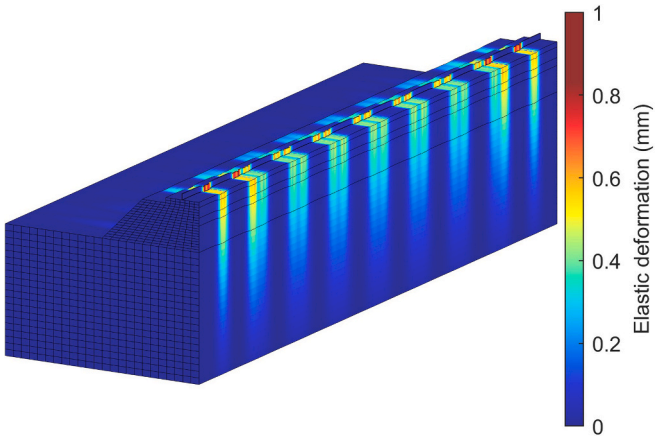

Fig. 2. An example of 3D track-ground elastic deformation (slice along track centreline). This example is intended for visualisation purposes only and does not reflect specific input values.

[37,39]. Several matrices necessary for evaluating train–track dynamic interactions are also precomputed. The empirical settlement equations are derived from the laboratory test data [40].

The differential settlement calculations are performed using an iterative approach in both the wavenumber-frequency and space–time domains. By incorporating the track irregularity profile, track compliance, and rolling stock characteristics, the dynamic interaction forces between the train and track are computed using a multi-body dynamic model. The combined stresses, including quasi-static, dynamic, and geostatic stress components, as well as the resulting settlements within the track and ground, are then evaluated along the entire track length, in alignment with the train's passage. After each axle passage, the vertical track geometry profile is updated, allowing a recalculation of the dynamic interaction forces and associated stresses for each subsequent iteration. This iterative process continues until either the specified number of cycles is reached or a predefined threshold value, as specified by railway maintenance standards (e.g., ballast tamping threshold), is met.

Due to the computational efficiencies achieved through precomputation, the iterative procedure requires significantly fewer computational resources, enabling rapid simulations across multiple axle passages [37]. This iterative approach is designed to simulate the evolution of differential settlement over time by sequentially updating the track geometry and associated loading conditions. The procedure is implemented across both the wavenumber-frequency and space–time domains and begins with the initial track geometry profile, track compliance, and rolling stock characteristics. These inputs are used within a train–track dynamic interaction model to compute the dynamic forces. The combined stress field, which include quasi-static, dynamic, and geostatic components, is then calculated using precomputed moving load transfer functions that incorporate nonlinear track-soil behaviour.

Using these stresses and empirical settlement equations (derived from laboratory data), the resulting settlements are computed at each location along the track. After each axle passage, the vertical geometry profile is updated, and the new profile is used to recalculate the dynamic interaction forces and stresses in the next iteration. This cycle repeats, updating the geometry and computing the standard deviation (SD) of the profile after each step. If the SD reaches or exceeds the predefined threshold for maintenance, a tamping intervention is performed to restore track quality. If the SD remains below the threshold, the process checks whether the cumulative traffic volume has reached a defined value. If not, the simulation continues with another iteration. If the defined traffic volume is reached and no maintenance is required, the simulation ends. This methodology can also be applied in the case of slab tracks, where maintenance requirements are higher.

Train-track dynamic interaction

A complete 2D vehicle model incorporating essential structural aspects of train dynamics [41] is employed to simulate rolling stock for predicting tamping interventions. Track-track dynamic interaction is modelled using a compliance method formulated within a dynamic reference frame aligned with the moving train [42,43]. The rolling stock considered is a passenger train, represented as a rigid multi-body vehicle featuring two suspension levels, illustrated in Fig. 3. Previous research by [6] has demonstrated that simplifying passenger vehicle models by reducing degrees of freedom can significantly increase errors when modelling differential settlement. The dynamic interaction analysis is conducted in the frequency domain, following the transformation of the track profile from the spatial domain. Equations (1)-(12) detail the formulation of dynamic interaction forces within this frequency domain. Hertzian stiffness is addressed through a linearisation method, in which only the static wheelset load is considered to obtain a representative stiffness value [44].

$$\{F_{dyn}(\Omega)\} = -\left([V] + [V^H] + [T]\right)^{-1}\{\Delta u(\Omega)\} \tag{1}$$

$$\{\Delta u(\Omega)\} = \delta u\{b(\Omega)\} \tag{2}$$

$$b(\Omega)_i = e^{i\frac{2\pi}{\lambda}a_i} \tag{3}$$

$$T(\Omega) = \frac{1}{2\pi}\int_{-\infty}^{+\infty} u_c^G(k_x,\omega)dk_x \tag{4}$$

$$V^H = \frac{1}{k_H} \tag{5}$$

$$k_H = \frac{3}{2G}{P_0}^{1/3} \tag{6}$$

$$V(\Omega) = [Z]\left([K^v] - \Omega^2[M^v]\right)^{-1}[Z]^T \tag{7}$$

$$[Z] = \begin{bmatrix} 0 & 0 & 0 & 0 & 0 & 0 & 1 & 0 & 0 & 0 \\ 0 & 0 & 0 & 0 & 0 & 0 & 0 & 1 & 0 & 0 \\ 0 & 0 & 0 & 0 & 0 & 0 & 0 & 0 & 1 & 0 \\ 0 & 0 & 0 & 0 & 0 & 0 & 0 & 0 & 0 & 1 \end{bmatrix} \tag{8}$$

In Equations (1)-(12), $F_{dyn}(\Omega)$ is the dynamic interaction forces in the frequency domain; Ω is the driving frequency, expressed as $\Omega = \frac{2\pi}{\lambda}v_0$; T is the flexibility term related to track compliance; δu is the vertical track irregularity amplitude, which is either taken from the initial input track geometry at the start of the simulation or from the updated geometry profile generated in the previous iteration during the settlement simulation process; a_i is the location of the contact point i; u_c^G is the Green's function of the vertical displacement at the contact point; V is the flexibility component associated with vehicle compliance; V^H is the contact flexibility matrix; k_H is the linearised Hertzian contact stiffness; P_0 is the static load transmitted from wheel to rail; G is a contact constant dependent on wheel radius and rail-wheel geometry; Z is a constant matrix; M^v is the vehicle mass matrix; and K^v is the vehicle stiffness matrix. The mass and stiffness matrices for the passenger vehicle, incorporating both primary and secondary suspension systems, are defined as follows:

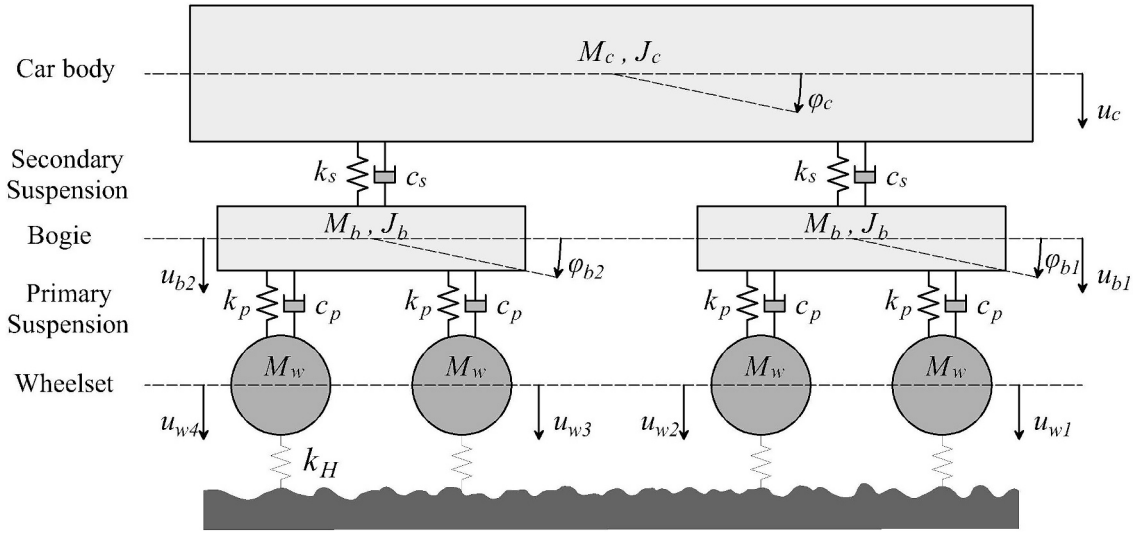

Fig. 3. Multi-body vehicle model.

$$[M^v] = \begin{bmatrix} Mc & 0 & 0 & 0 & 0 & 0 & 0 & 0 & 0 & 0 \\ 0 & Jc & 0 & 0 & 0 & 0 & 0 & 0 & 0 & 0 \\ 0 & 0 & Mb & 0 & 0 & 0 & 0 & 0 & 0 & 0 \\ 0 & 0 & 0 & Jb & 0 & 0 & 0 & 0 & 0 & 0 \\ 0 & 0 & 0 & 0 & Mb & 0 & 0 & 0 & 0 & 0 \\ 0 & 0 & 0 & 0 & 0 & Jb & 0 & 0 & 0 & 0 \\ 0 & 0 & 0 & 0 & 0 & 0 & Mw & 0 & 0 & 0 \\ 0 & 0 & 0 & 0 & 0 & 0 & 0 & Mw & 0 & 0 \\ 0 & 0 & 0 & 0 & 0 & 0 & 0 & 0 & Mw & 0 \\ 0 & 0 & 0 & 0 & 0 & 0 & 0 & 0 & 0 & Mw \end{bmatrix} \tag{9}$$

$$[K^v] = \begin{bmatrix} 2Ks & 0 & -Ks & 0 & -Ks & 0 & 0 & 0 & 0 & 0 \\ 0 & 2Ks \bullet lb^2 & -Ks \bullet lb & 0 & Ks \bullet lb & 0 & 0 & 0 & 0 & 0 \\ -Ks & -Ks \bullet lb & Ks + 2Kp & 0 & 0 & 0 & -Kp & -Kp & 0 & 0 \\ 0 & 0 & 0 & 2Kp \bullet lw^2 & 0 & 0 & -Kp \bullet lw & Kp \bullet lw & 0 & 0 \\ -Ks & Ks \bullet lb & 0 & 0 & Ks + 2Kp & 0 & 0 & 0 & -Kp & -Kp \\ 0 & 0 & 0 & 0 & 0 & 2Kp \bullet lw^2 & 0 & 0 & -Kp \bullet lw & Kp \bullet lw \\ 0 & 0 & -Kp & -Kp \bullet lw & 0 & 0 & Kp & 0 & 0 & 0 \\ 0 & 0 & -Kp & Kp \bullet lw & 0 & 0 & 0 & Kp & 0 & 0 \\ 0 & 0 & 0 & 0 & -Kp & -Kp \bullet lw & 0 & 0 & Kp & 0 \\ 0 & 0 & 0 & 0 & -Kp & Kp \bullet lw & 0 & 0 & 0 & Kp \end{bmatrix} \tag{10}$$

where *Mc* is the mass of the car body; *Mb* is the mass of the bogie; *Mw* is the mass of the wheelset; *Jb* is the rotational inertia of the car body; *Kp* is the complex stiffness associated with the primary suspension; *Ks* is the complex stiffness linked to the secondary suspension; *lb* is half the distance between the centres of gravity of adjacent bogies; and *lw* is half the wheelbase shared by wheels on the same bogie. Complex stiffness terms *Kp* and *Ks* are expressed as:

$$Kp = k_{pri} + i\omega c_{pri} \tag{11}$$

$$Ks = k_{sec} + i\omega c_{sec} \tag{12}$$

where k_{pri} and k_{sec} are the primary and secondary suspension spring stiffnesses, respectively, and c_{pri} and c_{sec} are the corresponding viscous damping coefficients.

Track irregularities can be characterised through their power spectral density (PSD) as a function of spatial frequency, for which various formulations exist. In this paper, the approach suggested by the Federal Railroad Administration (FRA) is employed, categorising tracks based on distinct irregularity levels to quantitatively assess unevenness [45]. The FRA-based formulation is defined by Equations (13)-(15):

$$S_n(k_x) = \frac{Ak_3^2\left(k_x^2 + k_2^2\right)}{k_x^4\left(k_x^2 + k_3^2\right)} \tag{13}$$

where the spatial frequency is $k_x = \frac{2\pi}{\lambda_{irr}}$, λ_{irr} is the irregularity wavelength, A is a roughness constant, k_2 and k_3 are spatial frequency constants.

Once the PSD is computed, the irregularity amplitude as a function of spatial frequency is derived by:

$$\delta u_j = \left(\sqrt{2S_n\left(k_{x_j}\right)\Delta k_x}\right) e^{-i\theta_j} \tag{14}$$

where Δk_x is the spatial frequency resolution and θ is the phase angle, assumed to be a random variable uniformly distributed within 0-2π. The use of a uniform distribution for the phase angle θ is a standard assumption in track irregularity generation because it reflects the random and uncorrelated nature of real-world geometric irregularities. This approach ensures that all phase values between 0 and 2π are equally likely, avoiding artificial periodicity or bias in the synthetic profile. While different distributions could theoretically lead to varying phase relationships, the uniform distribution reliably produces statistically valid and representative track geometry for engineering applications [45]. The metric for evaluating threshold exceedance is the standard deviation calculated over a 200 m track segment. The initial track profile

in terms of position x is established by summing contributions from all spatial frequencies as follows:

$$u_{irr}(x) = \sum_{j=1}^{N} \delta u_j e^{ik_{xj}x} \tag{15}$$

Fouled ballast settlement model

Large-scale triaxial cyclic loading tests were conducted by [40] using a large-scale triaxial testing setup equipped with a progressive wetting system at the University of South Carolina. The test focused on evaluating the impact of progressive wetting on the permanent deformation characteristics of fouled ballast materials sourced from three different sites. The study examined fouling indices (FI) of 23 and 40 under incremental moisture conditions. This paper adopts moisture levels ranging from 0 % to 6 % as representative case studies. The permanent strain from the initial loading cycles, during which rapid particle rearrangement occurs, was removed, and the cumulative deformation baseline was reset to zero for subsequent analysis.

Based on the experimental data, a ballast settlement prediction model is proposed to enhance the accuracy of tamping intervention forecasting. The model integrates the ballast fouling index (*FI*) and moisture content of fines (*w*) to capture their combined influence on ballast deformation. To ensure broader applicability across different track conditions and layers, the proposed settlement equation employs the ratio between the stress invariant quantity (t) and the Mohr–Coulomb failure criterion (t_{mc}). Additionally, the model uniquely incorporates cumulative settlement from previous axle passages into the calculation of incremental plastic deformation, rather than relying solely on the total number of load cycles, a limitation frequently seen in some conventional settlement prediction methods. This iterative approach provides distinct advantages, including improved representation of the nonlinear progression of ballast settlement and enhanced flexibility for modelling varying rates of track geometry deterioration under different axle load magnitudes. The computation of permanent strain within the model can be mathematically expressed as follows:

$$\Delta\varepsilon_{p\_b,i} = \alpha\left(\frac{t}{t_{mc}}\right)^{a} \times \left[\left(((dN \bullet i) + N_{lb})^{b} - 1\right) - \left(((dN \bullet (i-1)) + N_{lb})^{b} - 1\right)\right] \tag{16}$$

$$\alpha = (FI \bullet c)\left(d \bullet w + e \bullet w^2 + 1\right) \tag{17}$$

The corresponding settlement is then:

$$\Delta S_{b,i} = \sum_{j=1}^{k} \Delta\varepsilon_{p\_b,i_j} \bullet h_j \tag{18}$$

The term $\frac{t}{t_{mc}}$ defines the stress invariant quantity (t) and the Mohr–Coulomb failure criterion (t_{mc}) which can be calculated as follows:

$$t = \sqrt{2}\sqrt{J_2} \tag{19}$$

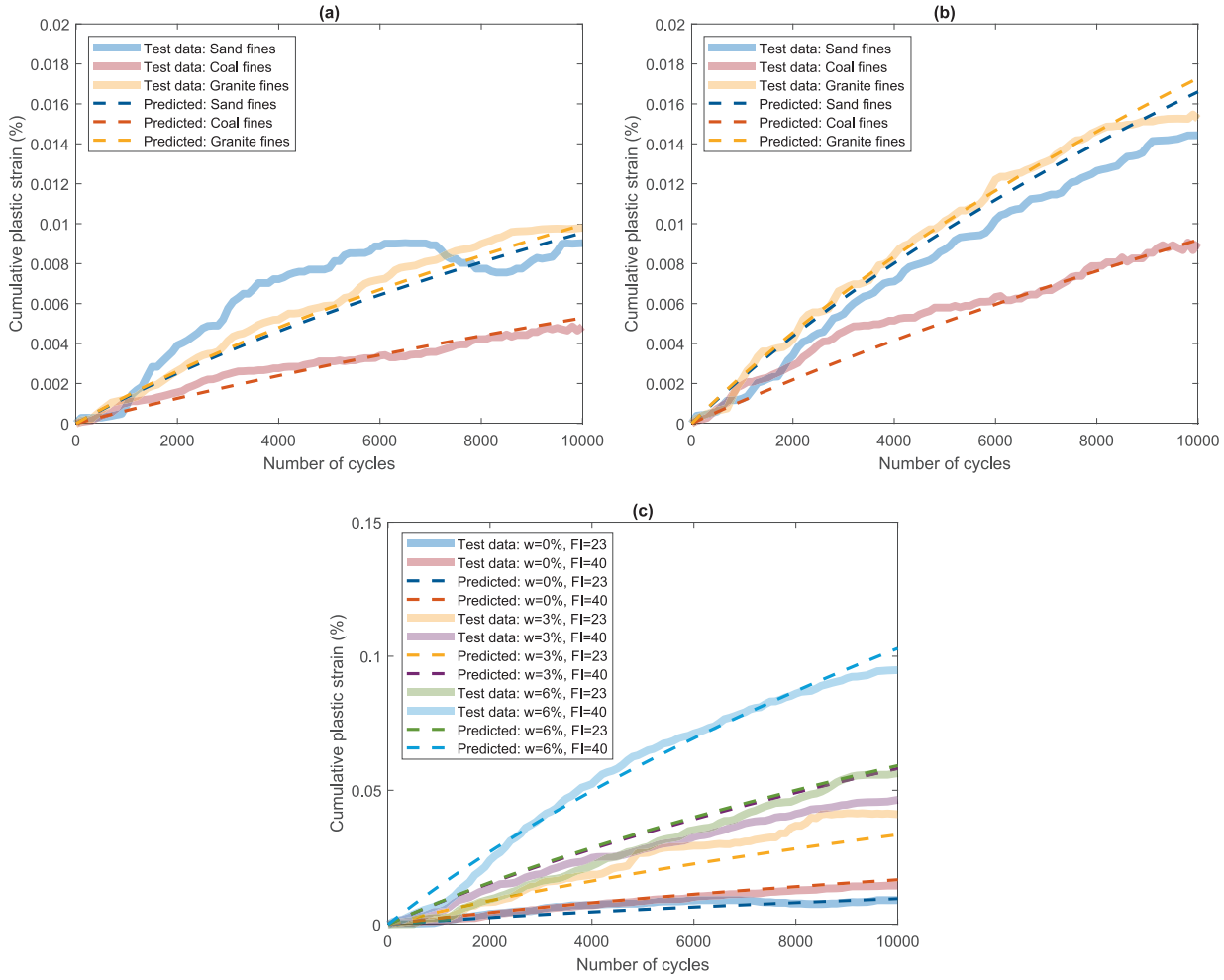

Fig. 4. Comparison of proposed ballast settlement model with experimental data: (a) different fouling materials (sand, coal, and granite fines) at FI = 23 and w = 0 % (b) different fouling materials (sand, coal, and granite fines) at FI = 40 and w = 0 % (c) Sand fines across different moisture contents and fouling indices.

$$t_{mc} = \frac{\sqrt{2}sin\varnothing' s' + \sqrt{6}cos\varnothing' c'}{sin\theta sin\varnothing' + \sqrt{3}cos\theta} \tag{20}$$

where θ is the lode angle, defined as:

$$\theta = -\frac{1}{3}sin^{-1}\left[\frac{3\sqrt{3}}{2}\left(\frac{J_3}{J_2^{3/2}}\right)\right] \tag{21}$$

where J_2 and J_3 are the 2nd and the 3rd invariant of deviatoric stress, defined as:

$$J_2 = \frac{1}{6}\left[\left(\sigma_1' - \sigma_2'\right)^2 + \left(\sigma_2' - \sigma_3'\right)^2 + \left(\sigma_3' - \sigma_1'\right)^2\right] \tag{22}$$

$$J_3 = \left(\sigma_1' - \sigma_m'\right)\left(\sigma_2' - \sigma_m'\right)\left(\sigma_3' - \sigma_m'\right) \tag{23}$$

where s' is the stress invariant quantity, defined as:

$$s' = \sqrt{3}\sigma_m' \tag{24}$$

where σ_m' is the mean effective stress, defined as:

$$\sigma_m' = \frac{\left(\sigma_1' + \sigma_2' + \sigma_3'\right)}{3} \tag{25}$$

where $\Delta\varepsilon_{p\_b,i}$ is ballast permanent strain increment; i is iterative step; N_{lb} is the number of load cycles since the last ballast renewal/tamping; $\Delta S_{b,i}$ is ballast settlement increment; h_j is the thickness of each layer; k is number of sublayers; dN is the frequency of load application; FI is ballast fouling index (%) where $FI \geq 23 \,\&\, FI \leq 40$; w is moisture of fines (%) where $w \leq 6$; $\varnothing'$ is friction angle; c' is cohesion; σ_1', σ_2', σ_3' are principal effective stresses; and a, b, c, d and e are empirical constants.

Fig. 4 presents a comparison between the proposed ballast settlement prediction model and experimental data, highlighting the influence of fouling index, moisture content, and fouling material type (sand, coal, and granite fines). Subfigures (a) and (b) demonstrate the model's ability to capture cumulative plastic strain trends for various fouling materials at FI = 23 and FI = 40, respectively, under dry conditions (w = 0 %). Subfigure (c) explores the impact of moisture and FI variations on sand fines, which is used in this paper as the baseline material. The empirical constants, represented as a, b, c, d and e, are: 2.15, 0.38, 0.00002, d = 0.0111 and 0.8, respectively. The results demonstrate that the proposed model accurately captures the measured ballast settlement behaviour. It should be noted that permanent strain measured during initial loading cycles was excluded from the analysis to avoid the influence of rapid particle rearrangements typical during early laboratory testing cycles. This ensures that the predictions are more representative of actual long-term track behaviour, enhancing their relevance and applicability for accurate tamping intervention planning. The model can be updated using new experimental data, allowing the development of a digital model of the real infrastructure to be studied.

Ballast moisture content and fouling type play critical roles in influencing long-term geometry degradation and the frequency of maintenance interventions. Moisture content reduces the shear strength of the ballast layer, especially under dynamic loading, which accelerates plastic deformation and settlement. This leads to faster growth in geometry SD, thus shortening tamping intervals. Similarly, fouling materials alter the mechanical behaviour of the ballast by affecting its friction angle and cohesion. The combined effects of fouling type and moisture content are incorporated into the settlement model are shown to significantly influence the deterioration rate of track geometry and maintenance planning, as demonstrated in later sections.

Track deterioration model calibration

The model's ability to simulate differential settlement progression under increasing axle passages was calibrated using historical track geometry data from railway track sections in the United Kingdom. Calibration involved analysis of the standard deviation of vertical track geometry measurements collected over 200-metre track lengths, specifically focusing on wavelengths ranging from 3 m to 35 m. The material properties for the site considered in Fig. 5, for the rails, rail pads, sleepers, ballast, sub-ballast, embankment, and subgrade are provided in Appendix A. This is also the site considered for the case studies in the next section.

According to site investigation data, the chosen section was characterised by a stiff subgrade. The traffic comprised entirely passenger trains, with associated vehicle parameters detailed in Appendix B. The annual traffic loading was approximately 13.66 million gross tonnes (MGT), and trains operated at a linespeed of 110 km/h. For validation purposes, vertical track geometry data obtained via a Track Recording Vehicle (TRV/TRC) over multiple measurement dates spanning June 2019 to September 2023 was used. No tamping interventions were performed during the considered period.

The initial geometric data recorded in June 2019 served as the baseline condition for the track deterioration model. Subsequently, the model simulated incremental geometry deterioration with each axle load passage up to September 2023. The progression of the track geometry standard deviation (SD) predicted by the model was compared with the actual measurement data obtained from the TRV, as illustrated

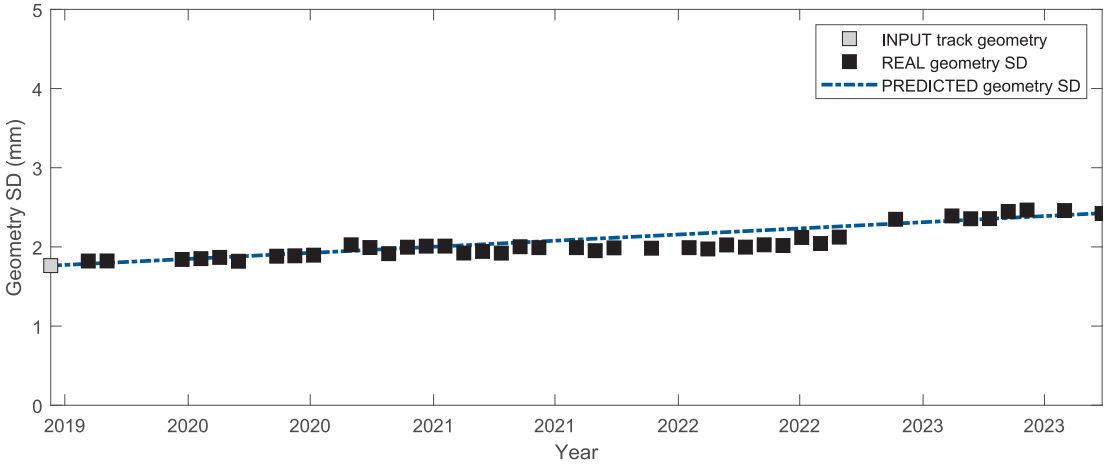

Fig. 5. Calibration of predicted vertical track geometry SD against field measurements over time.

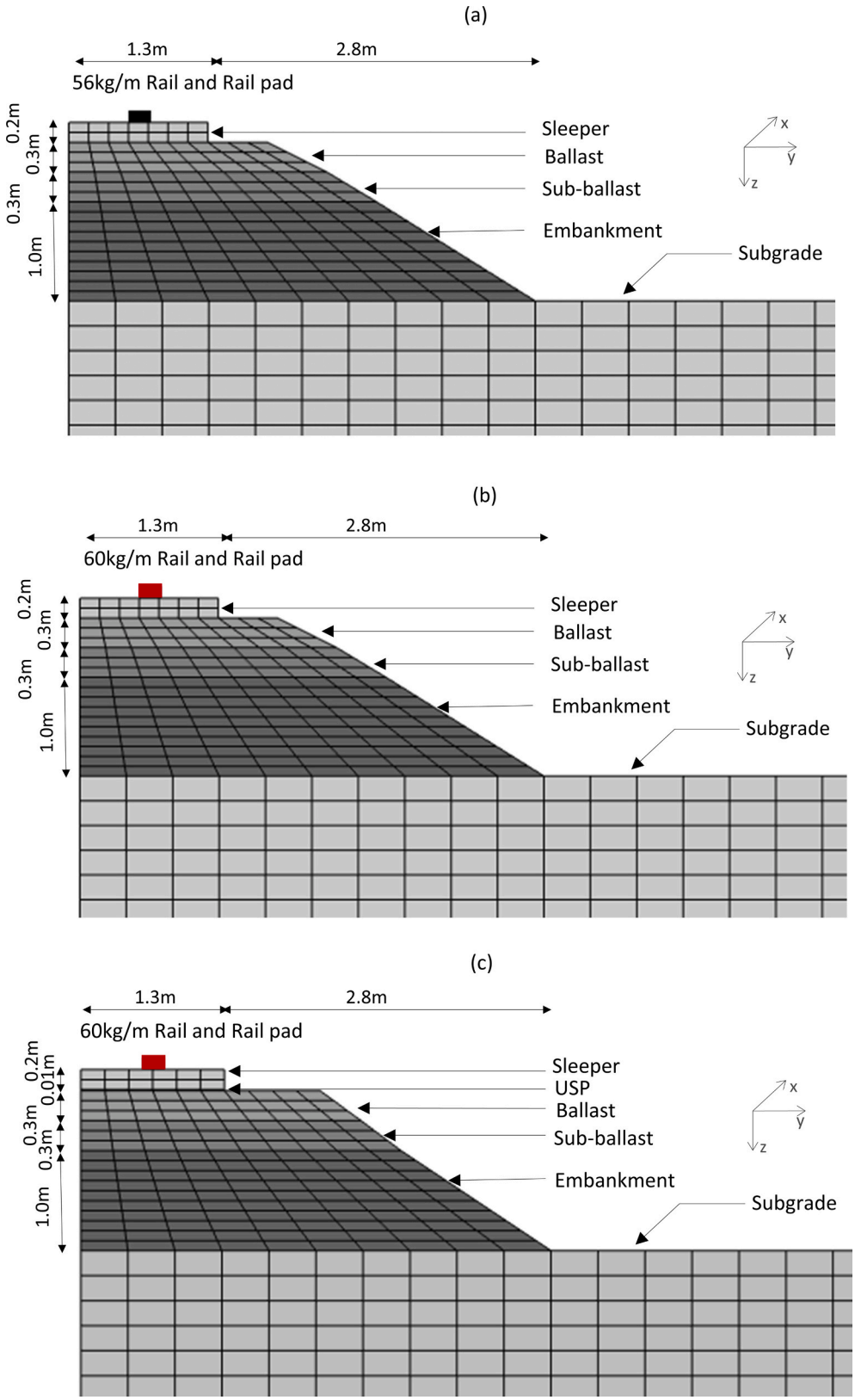

Fig. 6. Finite element meshes: (a) Standard track design with 56 kg/m rail (b) Standard track design with a heavier 60 kg/m rail (c) Standard track design but with a heavier 60 kg/m rail and USPs.

Table 1
Track properties for three track models.

Component	Parameter	(a)	(b)	(c)
Rail (single rail)	Type	56 kg/m	60 kg/m	60 kg/m
	Height (m)	0.159	0.172	0.172
	Length in transversal (m)	0.020	0.015	0.015
	Section area (m^2)	7.169×10^3	7.677×10^3	7.677×10^3
	Moment of Inertia y-y (m^4)	2.321×10^{-5}	3.038×10^{-5}	3.038×10^{-5}
	Moment of Inertia z-z (m^4)	0.422×10^{-5}	0.512×10^{-5}	0.512×10^{-5}
	Young's modulus (Pa)	2.11×10^{11}	2.11×10^{11}	2.11×10^{11}
	Density (kg/m^3)	7850	7850	7850
	Poisson's ratio	0.3	0.3	0.3
	Hysteric damping coefficient	0.01	0.01	0.01
Railpad (spring element)	Continuous stiffness (N/m^2)	250×10^6	250×10^6	250×10^6
	Viscous damping (Ns/m^2)	22.5×10^3	22.5×10^3	22.5×10^3
Sleeper (G44)	Height (m)	0.2	0.2	0.2
	Length in transversal (m)	2.5	2.5	2.5
	Sleeper spacing (m)	0.65	0.65	0.65
	Young's modulus (Pa)	3×10^{10}	3×10^{10}	3×10^{10}
	Density (kg/m^3)	2500	2500	2500
	Poisson's ratio	0.2	0.2	0.2
	Hysteric damping coefficient	0.01	0.01	0.01
USPs	Height (m)	–	–	0.01
	Young's modulus (Pa)	–	–	1.3×10^6
	Density (kg/m^3)	–	–	800
	Poisson's ratio	–	–	0
	Hysteric damping coefficient	–	–	0.08
Ballast	Height (m)	0.3	0.3	0.3
	Length in transversal (m)	3.2	3.2	3.2
	Young's modulus (Pa)	220×10^6	220×10^6	220×10^6
	Density (kg/m^3)	1600	1600	1600
	Poisson's ratio	0.12	0.12	0.12
	Hysteric damping coefficient	0.06	0.06	0.06
Sub-ballast (sand-gravel)	Height (m)	0.3	0.3	0.3
	Length in transversal (m)	n/a	n/a	n/a
	Young's modulus (Pa)	210×10^6	210×10^6	210×10^6
	Density (kg/m^3)	2000	2000	2000
	Poisson's ratio	0.3	0.3	0.3
	Hysteric damping coefficient	0.05	0.05	0.05
Embankment (sand-gravel)	Height (m)	1.0	1.0	1.0
	Young's modulus (Pa)	200×10^6	200×10^6	200×10^6
	Density (kg/m^3)	2000	2000	2000
	Poisson's ratio	0.3	0.3	0.3
	Hysteresis damping coefficient	0.05	0.05	0.05
Subgrade (clay/Silt)	Young's modulus (Pa)	75×10^6	75×10^6	75×10^6
	Density (kg/m^3)	2000	2000	2000
	Poisson's ratio	0.35	0.35	0.35
	Hysteric damping coefficient	0.03	0.03	0.03

in Fig. 5. The black rectangular markers indicate the measured geometry SD values at various dates, whereas the red rectangular marker represents the initial geometry SD in June 2019. The predicted evolution of geometry SD over axle passages is illustrated by the red dashed line. The settlement coefficients were tweaked to obtain a fit with the observed data thus calibrating the model. It is seen that the final model was able to accurately simulate the historical degradation at the site.

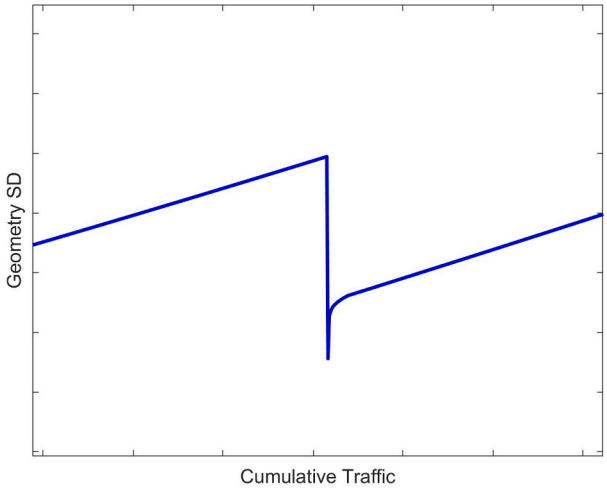

Fig. 7. Concept of SD growth after tamping.

Case studies

This section presents case studies used to evaluate the influence of various parameters on tamping intervention intervals. It is structured into three main aspects: track parameters, track geometry profile and traffic characteristics, and tamping intervention criteria.

Track parameters

Fig. 6(a)–(c) present the finite element meshes for three primary track models, with properties summarised in Table 1:

a) The standard track design used for the prior calibration, i.e. with 56 kg/m rail
b) The same standard track design but with a heavier 60 kg/m rail (larger bending stiffness)
c) The same standard track design but with a heavier 60 kg/m rail and Under Sleeper Pads

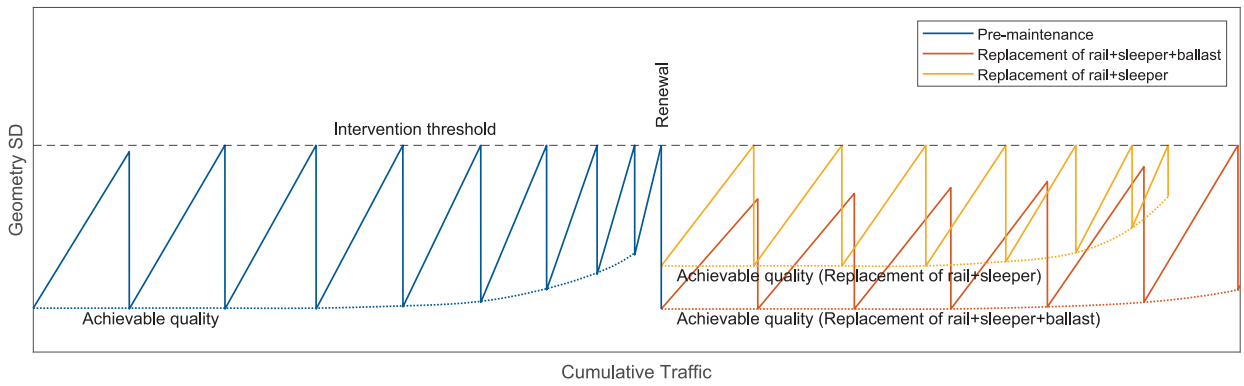

Fig. 8. Idealised pattern of tamping effects on track geometry (inspired by [8].

The cases are chosen to reflect two possible track renewal strategies. It is important to note that the track with 56 kg/m rail serves as the baseline for the analysis.

Track geometry profile and traffic parameters

The initial track irregularity profile is artificially generated using the Power Spectral Density (PSD) function, as specified by [45],

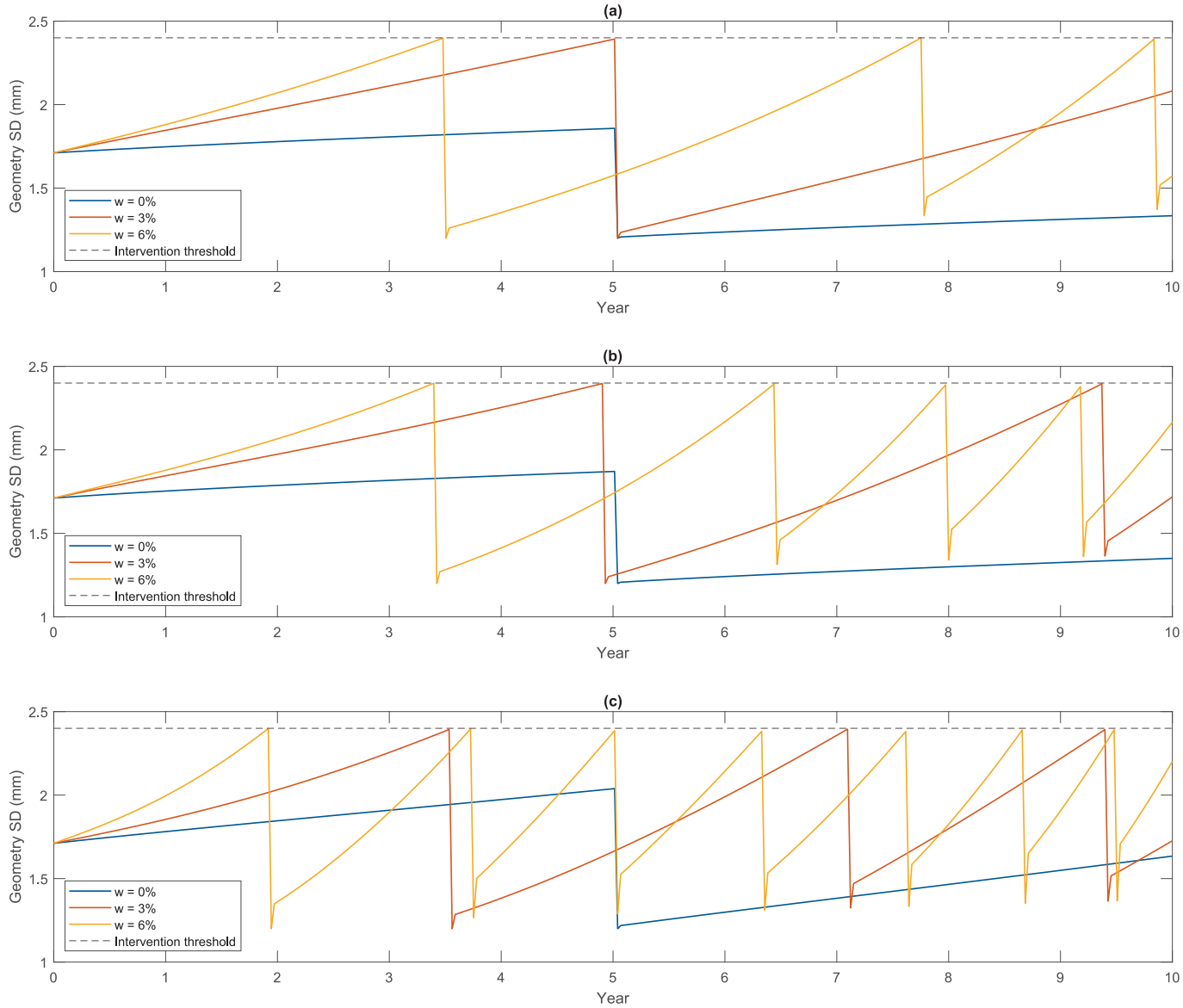

Fig. 9. Effects of moisture content on geometry SD and tamping interval: (a) train speed 130 km/h (b) train speed 160 km/h (c) train speed 200 km/h.

incorporating 40 frequency components. The parameters are defined as follows: $A = 0.45 \times 10^{-6}\,m^2 \bullet rad/m$, $k_2 = 14.639 \times 10^{-2}\,rad/m$, and $k_3 = 82.474 \times 10^{-2}\,rad/m$. These values result in a track geometry profile characterised by an initial standard deviation (SD) of 1.7 mm, indicating a level of track quality considered suitable for operational speeds of up to 200 km/h [46].

Three train speed scenarios are considered in the analysis: 130, 160, and 200 km/h. To ensure consistency and comparability between these speeds, the initial SD of 1.7 mm is consistently applied across all scenarios. It is assumed that the ballast has been subjected to prior traffic loading or dynamic track stabilisation to reduce the rapid initial rearrangement of ballast particles. The rolling stock used in the simulations is a passenger train, with its specifications detailed in Appendix B. To simulate the long-term progression of differential settlement, the model assumes a traffic volume of 17.5 million gross tonnes per annum (MGTPA), with the simulation period spanning ten years.

Tamping intervention

Tamping interventions are modelled based on assumptions that reflect typical maintenance practices and the expected effects on track geometry. The primary criterion for performing a tamping intervention is when the geometry SD over 200 m reaches a threshold of 2.4 mm. This threshold corresponds to a satisfactory quality band for linespeeds of up to 200 km/h. Alternatively, tamping is assumed to be carried out every five years as a preventive measure, whichever occurs first [47]. This dual criterion ensures that the track geometry is maintained within acceptable operational limits.

Following a tamping intervention on worn ballast, the geometry SD is assumed to decrease to approximately 1.2 mm, representing a 50 % improvement [8]. This reduction reflects the restoration of track geometry achieved through the tamping process, which repositions ballast particles and realigns the track structure.

After tamping, a period of rapid SD increase is anticipated due to the rearrangement of ballast stones, as they compact into a more stable configuration. This phase typically persists until approximately 2MGT of traffic has passed [8], after which the ballast reaches a resilient and stable state. This phenomenon, indicative of the track regaining its original resilient state, is illustrated in Fig. 7.

The condition of the ballast significantly influences the effectiveness of tamping operations. Specifically, tamping freshly laid ballast, particularly when ballast FI is relatively low, results in a better achievable geometry SD compared to tamping ballast that has experienced wear. Additionally, different renewal strategies can also influence the outcome. This discrepancy can be attributed to the enhanced compaction and stability of ballast following tamping, as illustrated in Fig. 8. The illustration highlights the geometry SD over time for three scenarios: pre-maintenance (blue line), replacement of rail + sleeper + ballast (red line), and replacement of rail + sleeper (orange line). The replacement of rail + sleeper + ballast option consistently achieves a lower geometry SD than the replacement of rail + sleeper option, indicating that the inclusion of ballast renewal further enhances the track quality. A degraded or contaminated ballast compromises the load distribution and reduces the effectiveness of tamping, leading to a rapid deterioration in track geometry. By contrast, ballast renewal restores the structural and elastic properties of the trackbed, allowing for more uniform compaction and significantly improving the initial geometry condition. This renewal approach not only achieves higher initial track quality but also slows the rate of deterioration, thereby extending the maintenance interval and improving overall track performance. In the present study, the deterioration rate following tamping is assumed to be 0.001 mm/MGT [8]. Regarding the renewal strategy, this study focuses on two specific scenarios: replacement of rail, and replacement of rail/sleeper/add USPs.

Table 2
Number of tamping intervals required at different water contents.

Water content (%)	Speed (km/h)	Number of tamping interventions required
0	130	1
3	130	1
6	130	3
0	160	1
3	160	2
6	160	4
0	200	1
3	200	3
6	200	7

Results and Analysis

This section presents the results and analysis of the effects of various operational and environmental factors on tamping intervals under consistent fouled ballast conditions (FI = 23, with a growth rate of 0.1 % per MGT). The analysis focuses on the influence of moisture content, train speed, traffic volume, ballast fouling type, and renewal strategy.

Effects of moisture content on tamping requirements

The influence of moisture content in the ballast layer on track geometry deterioration and the corresponding tamping requirements is investigated. Simulations are carried out for three train speeds: 130, 160, and 200 km/h, under varying moisture contents of 0 %, 3 %, and 6 %, with a constant traffic volume of 17.5MGTPA. Note that despite the variable train speeds under study, the train speed for all is 200 km/h, meaning the SD intervention threshold is 2.4 mm, thus enabling a direct comparison. The ballast is assumed to be fouled with sand particles. Fig. 9 illustrates the evolution of geometry standard deviation (SD) over a 10-year period. Table 2 summarises the corresponding number of tamping interventions required.

The analysis reveals that higher moisture content accelerates the degradation of track geometry. At each train speed, the geometry SD increases more rapidly as the moisture content increases, leading to more frequent tamping interventions. This effect is consistent across the speed scenarios, indicating moisture content has a significant impact on the ballast's ability to maintain stable track geometry.

At a train speed of 130 km/h (Fig. 9(a)), the geometry SD remains below the intervention threshold (2.4 mm) for both 0 % and 3 % moisture content throughout the 10-year period. Tamping, as indicated by a rapid drop in geometry standard deviation, is only performed every five years in accordance with the maintenance practice assumptions. This means that even though the geometry quality has not degraded to the intervention threshold, the maintenance cycle triggers the tamping process. In contrast, when the moisture content reaches 6 %, the geometry deterioration accelerates significantly, causing the SD to exceed the threshold around the third, seventh and ninth years, necessitating three tamping interventions within the 10-year period.

For the 160 km/h train speed (Fig. 9(b)), the number of tamping interventions required also increases with moisture content. At 0 % moisture, the geometry SD does not reach the threshold. At 3 % moisture content, the geometry degradation is faster, causing the SD to exceed the threshold after approximately four years, triggering tamping. Subsequently, an additional tamp occurs at the ninth year, making a total of two interventions. At the highest moisture content of 6 %, the deterioration rate increases further, resulting in four tamping interventions, with tamping conducted at approximately the third, sixth, eighth, and ninth years.

At the highest speed of 200 km/h (Fig. 9(c)), the impact of moisture content becomes even more pronounced. With 0 % moisture, the geometry SD still remains stable, and a tamping intervention only occurs at the fifth year. With 3 % moisture, the first intervention occurs around the third year when the threshold is reached, followed by tamping in the

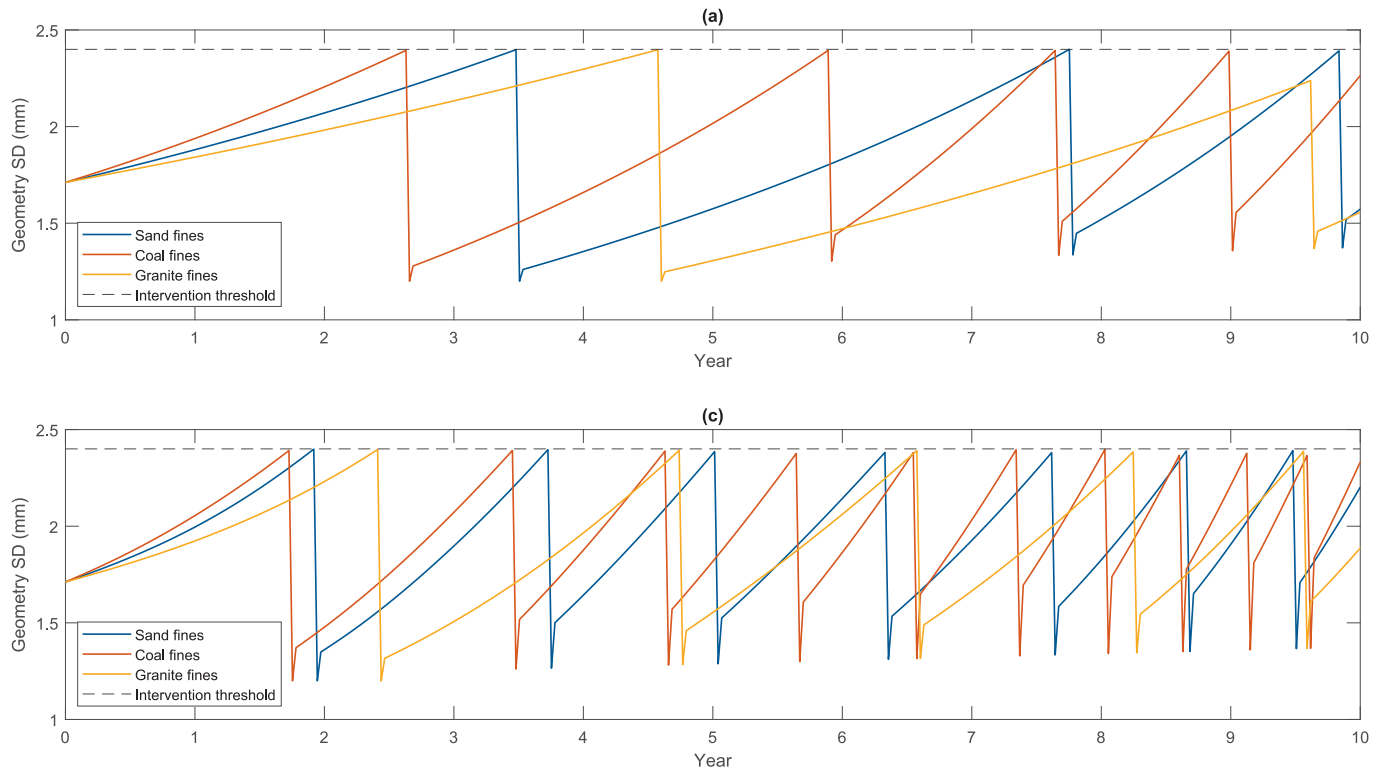

Fig. 10. Effects of ballast fouling types on geometry SD and tamping interval: (a) train speed 130 km/h (b) train speed 160 km/h (c) train speed 200 km/h.

Table 3
Number of tamping intervals required at different ballast materials and speeds.

Ballast fouling types	Speed (km/h)	Friction Angle (∅′)	Cohesion (c')	Number of tamping interventions required
Sand fines	130	36°	5 kPa	3
Coal fines	130	32°	15 kPa	4
Granite fines	130	40°	10 kPa	2
Sand fines	160	36°	5 kPa	4
Coal fines	160	32°	15 kPa	6
Granite fines	160	40°	10 kPa	2
Sand fines	200	36°	5 kPa	7
Coal fines	200	32°	15 kPa	10
Granite fines	200	40°	10 kPa	5

seventh and ninth years, resulting in three interventions. When the moisture content reaches 6 %, the geometry SD quickly reaches the intervention threshold within two years, requiring seven interventions over the 10-year period. This situation highlights the compounded effects of high speed and high moisture content on track geometry degradation.

Effects of ballast fouling types on tamping requirements

This section investigates the impact of different ballast fouling types on tamping intervals under a consistent water content of 6 % and a traffic volume of 17.5MGPA. The analysis covers three types of ballast fouling material: sand fines, coal fines and granite fines (i.e. from ballast particle abrasion), as shown in Fig. 10. The results are summarised in Table 3, which also identifies the friction angle and cohesion values associated with each fouling type. The analysis is conducted at three different train speeds: 130, 160, and 200 km/h.

Ballast fouling influences the rate of track geometry degradation due to its effect on the shear strength parameters of the ballast layer, particularly the friction angle and cohesion. The adopted values in this study are based on reported ranges from the literature and aim to reflect typical field conditions under moderate fouling severity and partial saturation [48–51]. Ballast with sandy fines is assumed to exhibit a relatively high friction angle of 36° and low apparent cohesion of 5 kPa. In contrast, coal dust fouling introduces finer, smoother, and more organic particles, which tend to reduce interparticle friction and increase cohesion when moist. Accordingly, a friction angle of 32° and cohesion of 15 kPa are adopted. Ballast fouled from aggregate breakdown (i.e. fines generated from ballast abrasion) maintains high interparticle friction due to the angular nature of the particles. Hence, a friction angle of 40° and apparent cohesion of 10 kPa are selected. The introduction of the apparent cohesion aims to simulate the interlocking effects.

At 130 km/h, the geometry SD increases at different rates depending on the ballast fouling type. The degradation rate of the ballast fouled due to sandy fines is relatively slow compared to other fouling types, resulting in three tamping interventions over the period. For the ballast fouled with coal fines, the lower friction angle leads to faster deterioration, requiring four interventions. For the ballast with fines due to abrasion, the combination of higher friction angle and moderate cohesion provides better stability, resulting in just two interventions. This shows that ballast aggregate breakdown has reduced impact on geometry degradation at low speeds due to its better interlocking properties.

At increased speed (160 km/h), dynamic loading accelerates geometry degradation for all ballast types. Four interventions are required for the ballast with sandy fines, as the geometry SD increases more rapidly compared to the 130 km/h case. Due to its lower friction angle, the geometry SD of ballast with the coal fines reaches the threshold more quickly, thus requiring six interventions over the period. Despite the increased speed, the enhanced friction angle helps maintain stability, limiting the interventions to three for the ballast fouled with fines from abrasion. The results indicate that at higher speeds, coal fines may pose a more significant problem compared to fines due to abrasion.

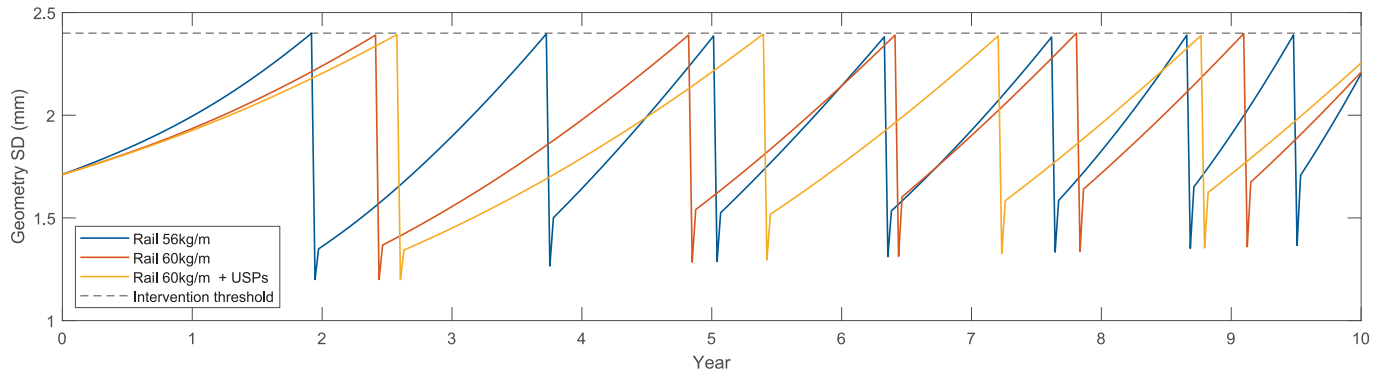

Fig. 11. Effects of renewal strategies on geometry SD and tamping interval.

Table 4
Number of tamping intervals required at different renewal strategies.

Ballast Materials	Speed (km/h)	Water content (%)	Number of tamping interventions required
Rail 56 kg/m	200	6	7
Rail 60 kg/m	200	6	5
Rail 60 kg/m + USPs	200	6	4

At the highest speed (200 km/h), the effect of ballast fouling becomes more pronounced. For the ballast with sand fines, the rapid degradation requires seven interventions, reflecting the high dynamic forces. The combination of low friction angle and high-speed results in the most frequent interventions, totaling ten for the ballast fouled with coal fines. For the ballast fouled due to abrasion, the superior mechanical properties of aggregate breakdown ballast reduce the intervention frequency to five. The results highlight that coal fouling is more problematic for lines with higher speeds, compared to fines due solely from abrasion. However, it is acknowledged that for higher train speeds, coal fouling is increasingly rare.

Effects of track renewal strategies on tamping requirements

The effects of different renewal strategies on tamping requirements are analysed under the following conditions: water content of 6 %, traffic volume of 17.5MGPA, and train speed of 200 km/h. Three renewal strategies are considered: 1) a standard track design with 56 kg/m rail, serving as the baseline, 2) the same standard track design but with a heavier 60 kg/m rail (larger bending stiffness), to assess the impact of increased rail stiffness and mass, 3) the same standard track design but with a heavier 60 kg/m Rail and USPs, to investigate the combined benefits of increased rail section and improved support conditions. These options are selected to reflect practical upgrade paths sometimes encountered in track renewal planning. The results are illustrated in Fig. 11 and summarised in Table 4.

Renewal strategies influence the future rate of track geometry degradation, as seen in Fig. 11. The choice of rail type, sleeper replacement, and addition of USPs collectively affect track settlement, thereby impacting the frequency of tamping interventions.

According to Table 4, the number of tamping interventions required varies significantly between the three renewal strategies. The track with the lighter 56 kg/m rail requires the most frequent tamping interventions, with a total of seven over the assessment period. This high intervention frequency is primarily due to the limited structural support and increased wear associated with the smaller rail section, resulting in more frequent crossings of the intervention threshold (2.4 mm), as seen in Fig. 11.

Upgrading the rail profile from 56 kg/m to 60 kg/m reduces the number of tamping interventions to five, which represents a 28.6 % reduction in tamping frequency. The enhanced bending stiffness and improved load distribution of the 60 kg/m rail help maintain track geometry more effectively via reducing ballast settlement. This indicates that modernising the rail profile alone can decrease maintenance frequency, even in the absence of further track-bed improvements.

The most comprehensive renewal strategy, which combines rail 60 kg/m with sleeper replacement and the addition of USPs, results in only four tamping interventions. This corresponds to a 42.9 % reduction compared to the baseline. The inclusion of USPs helps to reduce ballast degradation and provides resilient support under dynamic loading, thereby delaying the onset of geometry deterioration. As shown in Fig. 11, the standard deviation of geometry in this scenario remains consistently lower than in the other two strategies, demonstrating improved stability and load-bearing capacity.

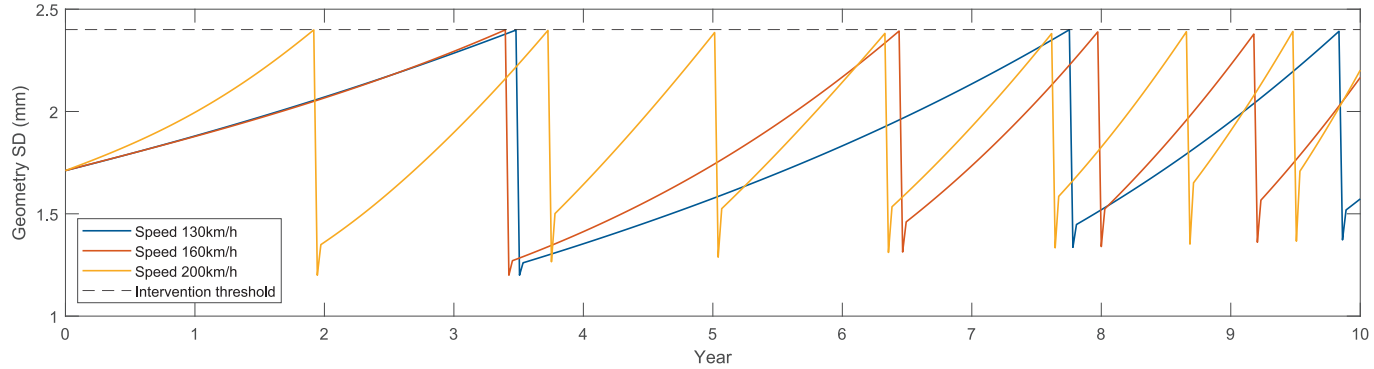

Fig. 12. Effects of train speeds on geometry SD and tamping interval.

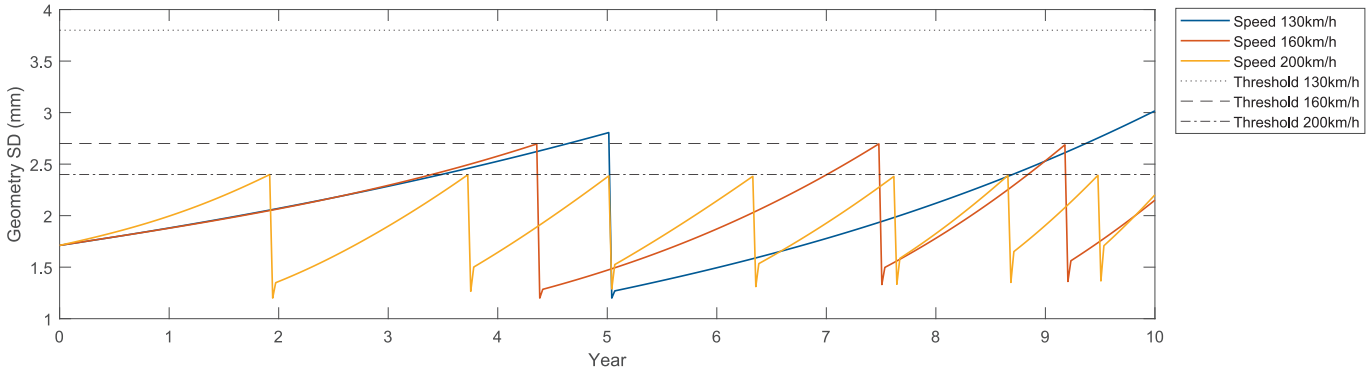

Fig. 13. Effects of train speeds on geometry SD and tamping interval (considering different speed thresholds).

Table 5
Number of tamping intervals required at different train speeds and SD thresholds.

Speed (km/h)	SD threshold (mm)	Number of tamping interventions required
130	2.4	3
160	2.4	4
200	2.4	7
130	3.8	1
160	2.7	3

Effects of train speed on tamping requirements

The influence of train speed on tamping intervals is analysed considering 6 % moisture content and a traffic volume of 17.5MGTPA. The results are illustrated in Fig. 12 and Fig. 13, while the number of tamping interventions required at different speeds and SD thresholds is summarised in Table 5. Fig. 12 presents the geometry SD progression over a 10-year period considering train speeds of 130, 160, and 200 km/h, using a uniform SD threshold of 2.4 mm to maintain a fair comparison.

The results indicate a clear trend of increasing geometry degradation as the train speed increases. This is consistent with the understanding that higher speeds exert greater dynamic forces on the track structure, leading to faster ballast degradation and settlement. The combination of high speed and elevated moisture content (6 %) significantly amplifies the geometry SD progression, as seen in both figures.

Fig. 12 shows that when a uniform threshold of 2.4 mm is used for all cases, the number of tamping interventions required increases with speed. At the lowest speed of 130 km/h, the track geometry reaches the intervention threshold three times over the period. For the medium speed of 160 km/h, the geometry deteriorates more rapidly, resulting in four tamping interventions. At the highest speed of 200 km/h, where the dynamic impact on the ballast is most severe, the number of tamping interventions rises to seven. These results highlight the significant influence of speed on maintenance requirements when a consistent

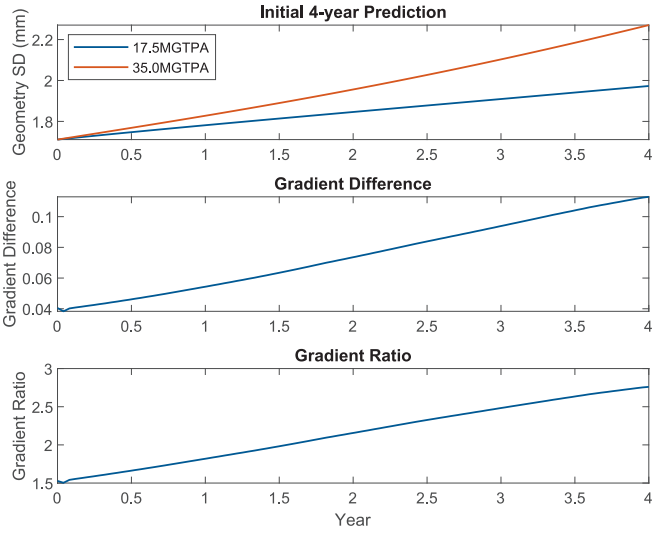

Fig. 15. Gradient difference and gradient ratio (17.5MGTPA vs 35.0MGTPA).

Table 6
Number of tamping intervals required at traffic volume.

Traffic (EMGTPA)	Speed (km/h)	Water content (%)	Number of tamping interventions required
17.5	200	0	1
35.0	200	0	2

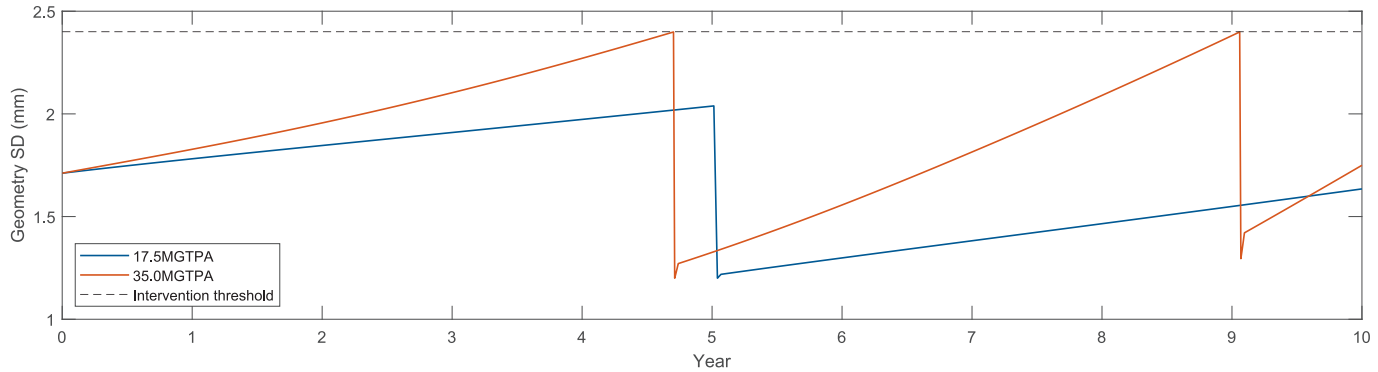

Fig. 14. Effects of traffic volume on geometry SD and tamping interval.

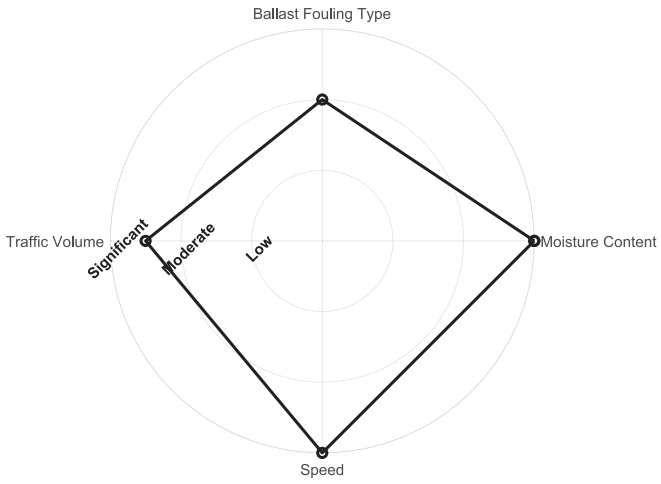

Fig. 16. Influence of key factors on ballast tamping requirements.

threshold is applied.

Fig. 13 shows the same train speed scenarios but also shows the SD thresholds commonly associated with the maximum train speeds at which these speeds would be permissible: 3.8 mm at 130 km/h, 2.7 mm at 160 km/h and 2.4 mm at 200 km/h. It is important to note that the 2.4 mm threshold is specifically appropriate for train speeds up to 200 km/h, while the higher thresholds for lower speeds reflect operational standards. In this study, the uniform 2.4 mm threshold is used primarily to ensure fair comparison between different speeds. At 130 km/h, the higher threshold of 3.8 mm results in only one tamping intervention over the period, compared to three interventions when using the uniform 2.4 mm threshold. Similarly, at 160 km/h with the threshold of 2.7 mm, only three tamping interventions are needed, compared to four when using the uniform threshold. For the 200 km/h speed, the number of tamping interventions remains unchanged at seven, as the threshold remains the same at 2.4 mm. This shows that linespeed-specific SD thresholds should be carefully chosen and reconfirms the importance of adopting intervention criteria that reflect operational conditions.

Effects of traffic volume on tamping requirements

The effect of traffic volume on tamping requirements is evaluated using two scenarios: low traffic (17.5MGTPA) and high traffic (35.0MGTPA). Both scenarios consider a train speed of 200 km/h and a moisture content of 0 %. The analysis is illustrated in Fig. 14 and Fig. 15, with the summary of the number of tamping interventions required shown in Table 6.

The results demonstrate that an increase in traffic volume significantly accelerates the degradation of track geometry. As shown in Fig. 14, the geometry SD increases more rapidly under high traffic conditions (35.0MGTPA) compared to low traffic (17.5MGTPA). This behaviour can be attributed to the increased cumulative loading and dynamic impact from a greater number of axle passages, leading to faster ballast settlement and increased track irregularities.

According to Table 6, at a traffic volume of 17.5MGPA, only one tamping intervention is required within the period. This indicates that the low traffic volume results in a relatively stable track geometry, where the gradual increase in SD remains within acceptable threshold limits. In contrast, when the traffic volume doubles to 35.0MGPA, the number of tamping interventions also doubles to two. The first intervention occurs at the fourth year when the geometry SD reaches the threshold of 2.4 mm. After tamping, the geometry condition improves, but the accelerated deterioration rate due to high traffic causes the SD to again reach the threshold around the ninth year, triggering a second tamping intervention. This pattern indicates a direct relationship between traffic volume and maintenance frequency, where higher traffic leads to more frequent interventions.

Fig. 15 provides a detailed analysis of the rate of geometry degradation by comparing the gradient difference and gradient ratio between two traffic load scenarios (17.5and 35.0MGT per annum). The gradient difference, defined as the absolute difference in degradation rates (i.e., the slope of SD increase) between high and low traffic cases, progressively increases over the four-year period, from approximately 0.04 mm/year initially to about 0.1 mm/year by year four. This rising difference indicates that the track under higher traffic deteriorates faster each year, reflecting additional dynamic loading effects. The gradient ratio, on the other hand, expresses the relative difference in degradation rate, calculated by dividing the high-traffic gradient by the low-traffic gradient. Initially around 1.5, it signifies that the degradation rate under 35.0MGT is 1.5 times that under 17.5MGT. This ratio increases steadily over time, approaching 3.0 by the fourth year. This increasing ratio indicates that the difference in degradation rate between the high and low traffic scenarios becomes more pronounced over time. The results imply that higher traffic volumes not only increase the immediate rate of deterioration but also cause the track to degrade more rapidly as the cumulative loading effect intensifies over time. This non-linear increase highlights the compounded impact of higher traffic levels on long-term track quality.

Understanding the impact of traffic volume on geometry degradation allows rail operators to better predict maintenance needs as traffic increases. This is particularly relevant for busy corridors, where higher loading intensifies track wear.

Discussion

It is evident that ballast tamping frequency requirements are governed by a complex interaction of moisture content, traffic volume, train speed, ballast fouling characteristics, and renewal plans. Among these, a constant elevated moisture content exerts a dominant effect, particularly in high dynamic loading environments, where elevated water levels reduce shear strength and lead to rapid ballast particle rearrangement. When combined with high train speed, this effect is further magnified due to increased dynamic loading. This highlights the critical importance of drainage management and minimising ballast fouling.

Ballast fouling type also influences track behaviour, although to a lesser extent. Fouling from coal fines, due to their lower friction angle and higher cohesion, induces greater settlement rates than abrasion-generated fines, which retain more interlock due to their angularity. As such, maintenance strategies should consider not just the fouling index, but if possible, also the fouling source. The analysis also demonstrates that traffic volume and train speed independently accelerate track deterioration, but their combined effect is non-linear and compounding. This is particularly clear in the gradient ratio analysis, which suggests that geometry degradation becomes progressively more severe with cumulative loading.

Fig. 16 summarises how the chosen heavily fouled site is influenced by the main variables under study. It is seen that ballast moisture content, train speed and traffic volume have a greater impact than ballast fouling type in terms of tamping requirements. These findings underscore the role of operational and environmental factors on maintenance planning. In particular it highlights the need for adequate track drainage and to minimise ballast fouling.

Conclusions

This paper presents a novel numerical framework for predicting future railway ballast tamping requirements by integrating an empirical ballast settlement model into a hybrid numerical simulation based on a 2.5D FEM-PML approach, calibrated using operational track geometry data. The approach is used to study the effect of ballast fouling material type, moisture content, speed, traffic volume and renewal strategies, providing a detailed understanding of track geometry degradation and

maintenance needs. Considering the case of a heavily fouled ballasted trackbed, the following conclusions are drawn:

1. An elevated ballast moisture content significantly accelerates geometry deterioration, thus increasing tamping requirements. At a constant 6 % ballast moisture content, the tamping frequency can more than double compared to dry conditions, particularly in the presence of high dynamic loading.
2. The type of ballast fouling material influences future tamping needs through its impact on shear strength. Coal fines, with lower friction angles, result in the highest intervention frequencies, whereas abrasion-generated fines provide more stable performance.
3. Track renewal strategies can play a key role in prolonging tamping intervals assuming the ballast is in reasonable condition. For example, for the studied site, upgrading from 56 kg/m to heavier 60 kg/m rails and adding USPs reduced the tamping requirements significantly, due to improved stiffness and load distribution.
4. For the same initial track geometry, higher train speeds increase the dynamic forces within the track structure, resulting in more rapid ballast settlement and geometry degradation.
5. Traffic volume has a non-linear effect on geometry degradation. For the case studied, although doubling the traffic from 17.5 to 35.0MGTPA approximately doubled the number of tamping interventions, the rate of geometry degradation increased disproportionately over time.

CRediT authorship contribution statement

C. Charoenwong: Writing – review & editing, Writing – original draft, Validation, Methodology, Formal analysis, Conceptualization. **D. P. Connolly:** Writing – review & editing, Writing – original draft, Validation, Resources, Conceptualization. **T. Wang:** Writing – review & editing, Conceptualization. **K. Liu:** Writing – review & editing. **P. Alves Costa:** Methodology. **A. Romero:** Writing – review & editing. **P. Galvín:** Writing – review & editing.

Declaration of competing interest

The authors declare that they have no known competing financial interests or personal relationships that could have appeared to influence the work reported in this paper.

Acknowledgements

The authors wish to thank Dr Yu Qian and Dr Shihao Huang for sharing the raw laboratory test data used to calibrate the settlement models. Network Rail are also thanked for sharing the track geometry data used for model validation. Finally, financial support from the Spanish Ministry of Science and Innovation under the research project PID2022-138674OB-C21 is acknowledged.

Appendix A. Track properties used for model validation

Component	Parameter	Value
Rail (single rail)	Type	56 kg/m rail
	Height (m)	0.159
	Length in transversal direction (m)	0.020
	Section area (m^2)	7.169×10^{3}
	Moment of Inertia y-y (m^4)	2.321×10^{-5}
	Moment of Inertia z-z (m^4)	0.422×10^{-5}
	Young's modulus (Pa)	2.11×10^{11}
	Density (kg/m^3)	7850
	Poisson's ratio	0.3
	Hysteresis damping coefficient	0.01
Railpad (spring element)	Continuous stiffness (N/m^2)	250×10^{6}
	Viscous damping (Ns/m^2)	22.5×10^{3}
Sleeper (G44)	Height (m)	0.2
	Length in transversal direction (m)	2.5
	Sleeper spacing (m)	0.65
	Young's modulus (Pa)	3×10^{10}
	Density (kg/m^3)	2500
	Poisson's ratio	0.2
	Hysteresis damping coefficient	0.01
Ballast	Height (m)	0.3
	Length in transversal direction (m)	3.2
	Young's modulus (Pa)	180×10^{6}
	Density (kg/m^3)	1600
	Poisson's ratio	0.25
	Hysteresis damping coefficient	0.06
Sub-ballast	Height (m)	0.25
	Length in transversal direction (m)	n/a
	Young's modulus (Pa)	210×10^{6}
	Density (kg/m^3)	2000
	Poisson's ratio	0.3
	Hysteresis damping coefficient	0.05
Embankment	Height (m)	1.0
	Young's modulus (Pa)	200×10^{6}
	Density (kg/m^3)	2000
	Poisson's ratio	0.3
	Hysteresis damping coefficient	0.05
Subgrade	Soil type	clay/silt
	Young's modulus (Pa)	120×10^{6}
	Density (kg/m^3)	2000
	Poisson's ratio	0.35
	Hysteresis damping coefficient	0.03

Appendix B. Passenger vehicle properties

Parameter	Value
Number of cars	11
Number of axles	44
Axle spacing (m)	2.9
Bogie spacing (m)	19
Car body mass (kg)	329×10^2
Car body pitching moment of inertia (kg.m^2)	208×10^4
Bogie mass (kg)	4932
Wheelset mass (kg)	1538
Bogie pitching moment of inertia (kg.m^2)	5150
Primary suspension stiffness (kNm^{-1})	3420
Primary suspension viscous damping (Nsm^{-1})	360×10^2
Secondary suspension stiffness (kNm^{-1})	1320
Secondary suspension viscous damping (Nsm^{-1})	360×10^2

Data availability

Data will be made available on request.

References

[1] Caetano LF, Teixeira PF. Predictive maintenance model for ballast tamping. J Transp Eng 2016;142. https://doi.org/10.1061/(ASCE)TE.1943-5436.0000825.

[2] Daddow M, Zhang X, Qiu H, Zhang Z, Liu Y. A mathematical model for ballast tamping decision making in railway tracks. Civil Eng J (Iran) 2020;6:2045–57. https://doi.org/10.28991/cej-2020-03091601.

[3] Martey EN. Modeling tamping recovery of track geometry using the copula-based approach; 2018.

[4] Guo Y, Markine V, Jing G. Review of ballast track tamping: mechanism, challenges and solutions. Constr Build Mater 2021. https://doi.org/10.1016/j.conbuildmat.2021.123940.

[5] Shi C, Fan Z, Connolly DP, Jing G, Markine V, Guo Y. Railway ballast performance: recent advances in the understanding of geometry, distribution and degradation. Transp Geotech 2023. https://doi.org/10.1016/j.trgeo.2023.101042.

[6] Charoenwong C, Connolly DP, Odolinski K, Alves Costa P, Galvín P, Smith A. The effect of rolling stock characteristics on differential railway track settlement: an engineering-economic model. Transp Geotech 2022;37:100845. https://doi.org/10.1016/j.trgeo.2022.100845.

[7] Chrismer, S., Hyslip, J., 2018. Principles of Degraded Ballast and Their Track Safety Implications, in: AREMA Annual Conference.

[8] Lichtberger B. Track compendium. PMC Media House; 2011.

[9] Charoenwong C, Connolly DP, Alves Costa P, Galvín P, Romero A. The effect of ballast moisture content and fouling index on railway track settlement. Transp Geotech 2024;45. https://doi.org/10.1016/j.trgeo.2024.101193.

[10] Docquier N, Lantsoght O, Dubois F, Brüls O. Modelling and simulation of coupled multibody systems and granular media using the non-smooth contact dynamics approach; n.d.. Doi: 10.1007/s11044-019-09721-0ï.

[11] Przybyłowicz M, Sysyn M, Gerber U, Kovalchuk V, Fischer S. Comparison of the effects and efficiency of vertical and side tamping methods for ballasted railway tracks. Constr Build Mater 2022;314. https://doi.org/10.1016/j.conbuildmat.2021.125708.

[12] Saussine Gilles, Azéma Emilien, Gautier PE, Peyroux Robert, Radjai F, Numerical FR, et al. Numerical modeling of the tamping operation by Discrete Element Approach; n.d.

[13] Tutumluer Erol, Huang Hai, Assistant GR, Hashash Youssef, Ghaboussi Jamshid, et al. Aggregate Shape Effects on Ballast Tamping and Railroad Track Lateral Stability; 2006.

[14] Lamprea-Pineda AC, Connolly DP, Hussein MFM. Beams on elastic foundations – a review of railway applications and solutions. Transp Geotech 2022;33:100696. https://doi.org/10.1016/j.trgeo.2021.100696.

[15] Wilk S, Li D, DeVencenty D. Relationship of Inspection Methods to Ballast Degradation Models: Phase II; 2024.

[16] de Miguel A, Lau A, Santos I. Numerical simulation of track settlements based on an iterative holistic approach. J Braz Soc Mech Sci Eng 2018;40. https://doi.org/10.1007/s40430-018-1300-8.

[17] Grossoni I, Powrie W, Zervos A, Bezin Y, Le Pen L. Modelling railway ballasted track settlement in vehicle-track interaction analysis. Transp Geotech 2021;26:100433. https://doi.org/10.1016/j.trgeo.2020.100433.

[18] Kumar N, Kossmann C, Scheriau S, Six K. An efficient physical-based method for predicting the long-term evolution of vertical railway track geometries. Proc Inst Mech Eng F J Rail Rapid Transit 2021. https://doi.org/10.1177/09544097211024803.

[19] Nielsen JCO, Li X. Railway track geometry degradation due to differential settlement of ballast/subgrade – numerical prediction by an iterative procedure. J Sound Vib 2018;412:441–56. https://doi.org/10.1016/j.jsv.2017.10.005.

[20] Charoenwong C, Connolly DP, Dong K, Alves Costa P, Soares PJ, Woodward PK. A multi-model approach to analyse railway track-ground dynamics and soil nonlinearity. Lect Notes Civil Eng 2022;165:37–48. https://doi.org/10.1007/978-3-030-77234-5_4.

[21] Chumyen P, Connolly DP, Woodward PK, Markine V. A comparison of earthwork designs for railway transition zones. Constr Build Mater 2023;395. https://doi.org/10.1016/j.conbuildmat.2023.132295.

[22] Chumyen P, Connolly DP, Woodward PK, Markine V. The effect of soil improvement and auxiliary rails at railway track transition zones. Soil Dyn Earthq Eng 2022;155:107200. https://doi.org/10.1016/j.soildyn.2022.107200.

[23] Connolly DP, Dong K, Alves Costa P, Soares P, Woodward PK. High speed railway ground dynamics: a multi-model analysis. Int J Rail Transport 2020;8:324–46. https://doi.org/10.1080/23248378.2020.1712267.

[24] Lamprea-Pineda AC, Connolly DP, Castanheira-Pinto A, Alves-Costa P, Hussein MFM, Woodward PK. On railway track receptance. Soil Dyn Earthq Eng 2024;177:108331. https://doi.org/10.1016/j.soildyn.2023.108331.

[25] Chen C, McDowell GR. An investigation of the dynamic behaviour of track transition zones using discrete element modelling. Proc Inst Mech Eng F J Rail Rapid Transit 2016;230:117–28. https://doi.org/10.1177/0954409714528892.

[26] Dahlberg T. Some railroad settlement models – a critical review. Proc Inst Mech Eng F J Rail Rapid Transit 2001;215:289–300. https://doi.org/10.1243/0954409011531585.

[27] Guo Y, Zhao C, Markine V, Jing G, Zhai W. Calibration for discrete element modelling of railway ballast: a review. Transp Geotech 2020;23:100341. https://doi.org/10.1016/j.trgeo.2020.100341.

[28] Shih JY, Grossoni I, Bezin Y. Settlement analysis using a generic ballasted track simulation package. Transp Geotech 2019;20:100249. https://doi.org/10.1016/j.trgeo.2019.100249.

[29] Indraratna B, Nimbalkar S. Stress-strain degradation response of railway ballast stabilized with geosynthetics. J Geotech Geoenviron Eng 2013;139:684–700. https://doi.org/10.1061/(asce)gt.1943-5606.0000758.

[30] Li D, Selig ET. Cumulative plastic deformation for fine-grained subgrade soils. J Geotech Eng 1996;122:1006–13. https://doi.org/10.1061/(asce)0733-9410(1996)122:12(1006).

[31] Li D, Selig ET. Resilient modulus for fine-grained subgrade soils. J Geotech Eng 1994;120:939–57.

[32] Ramos A, Gomes Correia A, Indraratna B, Ngo T, Calçada R, Costa PA. Mechanistic-empirical permanent deformation models: laboratory testing, modelling and ranking. Transp Geotech 2020;23. https://doi.org/10.1016/j.trgeo.2020.100326.

[33] Alves Costa P. Vibrações do sistema via-maciço induzidas por tráfego ferroviário. Modelação numérica e validação experimental; 2010.

[34] Karlström A, Boström A. An analytical model for train-induced ground vibrations from railways. J Sound Vib 2006;292:221–41. https://doi.org/10.1016/j.jsv.2005.07.041.

[35] Knothe K, Wu Y. Receptance behaviour of railway track and subgrade. Arch Appl Mech 1998;68:457–70. https://doi.org/10.1007/s004190050179.

[36] Montagna M. Train induced ground vibration: a hybrid time and frequency domain modelling technique. Politecnico di Milano; 2011.

[37] Charoenwong C, Connolly DP, Woodward PK, Galvín P, Alves Costa P. Analytical forecasting of long-term railway track settlement. Comput Geotech 2022;143:104601. https://doi.org/10.1016/j.compgeo.2021.104601.

[38] Charoenwong C, Connolly DP, Woodward PK, Galvín P, Alves Costa P. Numerical modelling of the evolution of differential settlement of railway tracks. In: Eleventh International Conference on the Bearing Capacity of Roads, Railways and Airfields, Volume 3. CRC Press; 2022. p. 291–300. https://doi.org/10.1201/9781003222910-30.

[39] Chonlatis Charoenwong. Numerical Simulation of Differential Railway Track Settlement. University of Leeds, Leeds; 2024.

[40] Huang S, Qian Y. Effect of progressive wetting on permanent deformation of fouled ballast under cyclic loading. Can Geotech J 2024.

[41] Zhai W, Cai Z. Dynamic interaction between a lumped mass vehicle and a discretely supported continuous rail track. Comput Struct 1997;63:987–97. https://doi.org/10.1016/S0045-7949(96)00401-4.
[42] Colaço A, Costa PA, Connolly DP. The influence of train properties on railway ground vibrations. Struct Infrastruct Eng 2016;12:517–34. https://doi.org/10.1080/15732479.2015.1025291.
[43] Costa PA, Calçada R, Cardoso AS. Influence of train dynamic modelling strategy on the prediction of track-ground vibrations induced by railway traffic. Proc Inst Mech Eng F J Rail Rapid Transit 2012;226:434–50. https://doi.org/10.1177/0954409711433686.
[44] Kouroussis G, Connolly DP, Verlinden O. Railway-induced ground vibrations – a review of vehicle effects. Int J Rail Transport 2014;2:69–110. https://doi.org/10.1080/23248378.2014.897791.
[45] Federal Railroad Administration. Statistical Representations of Track Geometry : Volume I. Washington, D.C.; 1980.
[46] Network Rail. Track geometry - Inspections and minimum actions - NR/L2/TRK/001/mod11. London, UK; 2015.
[47] Neuhold, J. Tamping within sustainable track asset management. Verlag d. Technischen Universität Graz; 2020.
[48] Dissanayake G, Kurukulasuriya LC, Dissanayake PBR. Effect of Rail Track Ballast Degradation on Shear Strength. In: International Conference on Geotechnical Engineering (ICGE). Colombo; 2015.
[49] Huang H, Tutumluer E, Dombrow W. Laboratory characterization of fouled railroad ballast behavior. Transp Res Rec 2009;93–101. https://doi.org/10.3141/2117-12.
[50] Ramadan AN, Zhang J, Li T, Xu B, Jing P. the impact of sandy fouled ballast properties on its mechanical behavior. Int J Civil Infrastruct 2024;07. https://doi.org/10.11159/ijci.2024.015.
[51] Tutumluer E, William D, Hai H. Laboratory characterization of coal dust fouled ballast behaviour. In: AREMA 2008 Annual Conference & Exposition. Salt Lake City; 2008.